Volume 15
Number 38
14 October 2023
Pages 15437-15872

Nanoscale

rsc.li/nanoscale

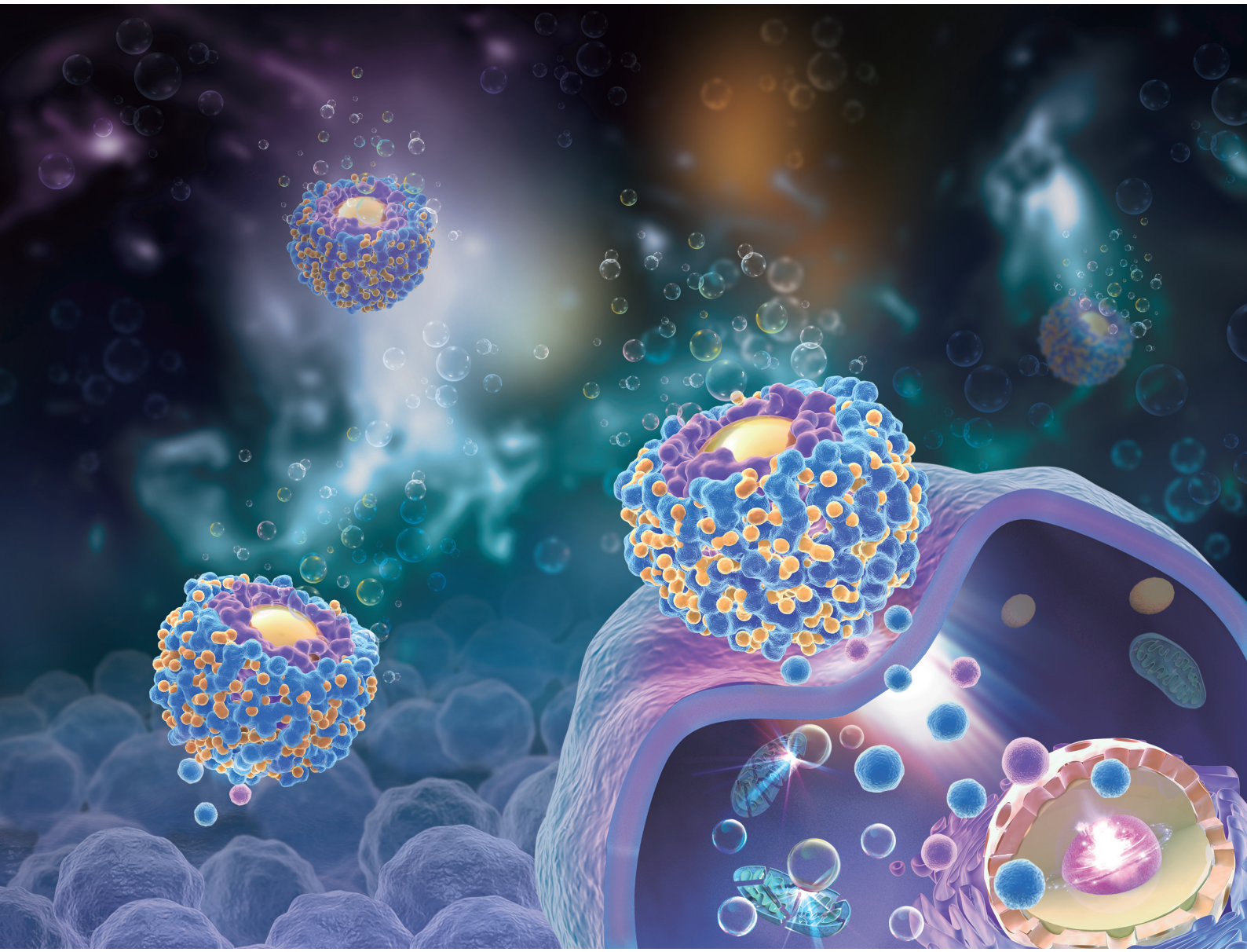

ISSN 2040-3372

ROYAL SOCIETY OF CHEMISTRY

PAPER

Wenjuan Liu, Bohan Wang *et al.*
A drug co-delivery platform made of magnesium-based micromotors enhances combination therapy for hepatoma carcinoma cells

NCNST

Nanoscale

PAPER

View Article Online
View Journal | View Issue

Cite this: *Nanoscale*, 2023, **15**, 15573

A drug co-delivery platform made of magnesium-based micromotors enhances combination therapy for hepatoma carcinoma cells†

Qingtao Song,‡[a,b] Yilin Liu,‡[a,b] Xiaoyong Ding,[a] Miao Feng,[a] Jing Li,[c] Wenjuan Liu,*[a,b] Bohan Wang*[d] and Zhongwei Gu[a]

Combination therapy is an emerging strategy to overcome multidrug resistance (MDR) in hepatocellular carcinoma (HCC) chemotherapy treatment. However, the passive diffusion in traditional delivery systems greatly retards the approach and penetration of drugs into hepatocellular carcinoma cells and thus hinders the efficacy of combination therapy. Micro/nanomotors with autonomous locomotion in a tiny scale provide the possibility of tackling this issue. Herein, an active drug delivery micromotor platform delicately designed to load drugs with different physicochemical properties and enhance the drug permeability of cells is demonstrated for HCC chemotherapy treatment. The biocompatible micromotor platform Mg/PLGA/CHI comprised magnesium (Mg) coated with two polymer layers made of poly(lactic-*co*-glycolic acid) (PLGA) and chitosan (CHI), where the hydrophobic and hydrophilic drugs doxorubicin (Dox) and Curcumin (Cur) were loaded, respectively. The autonomous motion of the micromotors with velocity up to 45 μm s^{-1} greatly enhanced the diffusion of chemotherapeutic drugs and led to higher extracellular and intracellular drug distribution. Moreover, hydrogen produced during the motion eliminated the excess reactive oxygen species (ROS) in the human hepatocellular carcinoma (HepG2) cells. Compared with inert groups, the absorption of Dox and Cur from the active micromotors was about 2.9 and 1.5 times higher in human hepatocellular carcinoma (HepG2) cells. In addition, the anti-tumor activity also obviously improved at the micromotor concentration of 1 mg mL^{-1} (cell proliferation was reduced by almost 30%). Overall, this work proposes an approach based on loading different chemotherapy agents on an active delivery system to enhance drug permeability and overcome MDR and provides a potentially effective therapeutic strategy for the treatment of HCC.

Received 3rd April 2023,
Accepted 14th August 2023

DOI: 10.1039/d3nr01548c

rsc.li/nanoscale

Introduction

Hepatocellular carcinoma (HCC) has emerged as a leading cause of cancer-related death among cancer patients globally. It is the most common type of primary liver cancer with high prevalence and high burden of morbidity and hence has gained increasing attention in recent years.[1–3] In addition, due to the lack of typical symptoms during the early stage of HCC, the majority of HCC patients are diagnosed at advanced stages. Thus, an effective non-surgical treatment is urgently needed. Drugs, such as doxorubicin (Dox), sorafenib, 5-fluorouracil, and cisplatin, serve as clinical chemotherapy medication.[4,5] However, they have very limited therapeutic effects (only 10% response rates) in the treatment of HCC, which may be caused by the development of multidrug resistance (MDR) to chemotherapy.[6] Combination therapy is recently emerging as a strategy for cancer therapy to address this issue. Specifically, the combination of chemotherapy drugs with chemosensitizers would regulate different signalling pathways in cancer cells; the multidrug resistance problem can be alleviated in this way, and further, the therapeutic effect would maximize, and side effects would reduce.[7]

The selection of drug combinations with different modes of action can effectively stop the development of multi-drug resistance in cancer cells.[8] Dox, a common anti-HCC chemotherapy

[a]*Research Institute for Biomaterials, Tech Institute for Advanced Materials, College of Materials Science and Engineering, Nanjing Tech University, Nanjing 211816, China. E-mail: liuwenjuan@njtech.edu.cn*
[b]*Jiangsu Collaborative Innovation Center for Advanced Inorganic Functional Composites, Nanjing Tech University, Nanjing 211816, China*
[c]*Key Laboratory of Biomass Chemical Engineering of Ministry of Education, College of Chemical and Biological Engineering, Zhejiang University, Hangzhou 310027, China*
[d]*Department of Urology, The Second Affiliated Hospital, School of Medicine, Zhejiang University, Hangzhou 310000, China. E-mail: wangbohan@zju.edu.cn*
†Electronic supplementary information (ESI) available. See DOI: https://doi.org/10.1039/d3nr01548c
‡These authors contributed equally to this work

medication, causes deoxyribonucleic acid (DNA) damage in cells and activates apoptosis of cancer cells, leading to programmed death.[9] However, the clinical application of Dox is limited due to its critical cardiotoxicity and low response rate owing to multidrug resistance. Curcumin (Cur) is a traditional bioactive constituent found in the perennial herb *Curcuma longa*.[10] Cur is an effective sensitizer that can limit the activity of proteins related to drug resistance and restrict cancer cells from proliferating.[11] At the same time, Cur exerts some anti-angiogenic effect such that palingenetic tumor blood vessels restrict tumor invasion.[12] Therefore, we hypothesize that the combination of Dox and Cur would be an effective strategy for enhancing the therapeutic efficacy of Dox.[5] Apart from these benefits, improving drug permeability and retention in Hepatocellular carcinoma cells is also extremely important. At present, drug carriers used for combined passive drug delivery mainly include nanoparticles,[13] polymer micelles,[14] hydrogels[15] and microneedles,[16] which are incapable of enhancing the drug transport efficiency and permeability.

Artificial micro/nanomotors capable of transforming different forms of energies (chemical or physical energies) into mechanical motion,[17,18] have garnered significant attention for their promising biomedical applications, such as active drug delivery,[19] diagnosis,[20] and minimally invasive surgery,[21] over the past decades. Especially, due to their inherent capabilities like self-motion and efficient cargo transport, micro/nanomotors can serve as active drug delivery vectors to enhance drug permeability and retention in cancer cells.[22–24] Compared with traditional nanomedicine delivery systems that rely on passive transport, micromotors based on diverse motion patterns transport drugs in a more efficient way. Among them, chemical-propelled micro/nanomotors offer greater driving forces and avoid the installation of complex external fields.[25–28] Recently, magnesium (Mg)-based micromotors have been synthesized to deliver drugs *in vivo* as they can react with biofluids to produce hydrogen for propulsion.[29–31] Being a necessary trace element for human body, Mg is biocompatible, and its degradation product in the physiological environment is harmless to tissues and cells.[30,32] To date, diverse micromotors have demonstrated the possibility of co-drug delivery.[29,33,34] However, developing a micromotor that can be synergistically administered with clinical drugs possessing different physicochemical properties remains a huge challenge.

In this work, we present a new strategy based on a self-propelled Mg micromotor that combines active transport and co-drug delivery to intensify the chemotherapy efficiency. Specifically, this Mg-based micromotor was fabricated by using a Mg microparticle as the core along with a biodegradable polymer poly(lactic-*co*-glycolic acid) (PLGA) and the natural biocompatible polysaccharide chitosan (CHI) as asymmetrical coating layers to ensure superior biocompatibility of the drug delivery system. Meanwhile, both hydrophobic Dox and hydrophilic Cur were respectively loaded on the PLGA and CHI coating layers. The micromotor could react with the cell culture medium and propel autonomously to enhance drug permeability and adsorption in the cancer cells. Due to the powerful motion of these micromotors, the common chemotherapy drug (Dox) and the popular sensitizer (Cur) could permeate into the cells to potentiate a synergistic effect. Simultaneously, hydrogen produced during the motion led to reactive oxygen species (ROS) scavenging. Therefore, obvious proliferation inhibition and cell apoptosis were achieved in the micromotor groups when they were co-incubated with human hepatocellular carcinomas (HepG2) cells in contrast to the inert groups. Overall, our work successfully demonstrates an active drug delivery system that accomplishes synergistic chemotherapy *via* loading different chemotherapeutic drugs and autonomous locomotion, showcasing promising application potential in HCC treatment.

Results and discussion

In recent years, combined drug therapy has become an effective alternative to single drug therapy as it enhances the therapeutic effect due to the collective action of two different drugs at specific drug concentrations in the tumor environment.[13–15,35] For the chemotherapy of HCC, an active combined drug delivery system made of a Mg-based micromotor was developed. As shown in Fig. S1,† the preparation process of the Mg/PLGA/CHI micromotor drug delivery platform was simple and repeated. The drugs Dox and Cur could be easily embedded and adjusted in the CHI and PLGA layers, respectively. Notably, Dox is one of the most effective drugs for liver cancer, and Cur is an effective sensitizer that can limit the activity of proteins related to drug resistance and restrict cancer cells from proliferating.[5,11] Due to the autonomous propulsion of the micromotor, active administration of two drugs to the hepatic tumor would be achieved, which can greatly improve the efficiency of HCC treatment. Significantly, combination chemotherapy and active drug delivery can overcome multidrug resistance and boost the permeability of drugs in HepG2 cells. Simultaneously, H_2 generation during Mg-based micromotor motion eliminates ROS in the tumor microenvironment and inhibits tumor cell proliferation (Scheme 1).

The fabrication steps of the Dox/Cur-loaded Mg-based micromotors are schematically illustrated in Fig. S1.† With the asymmetrical and uniform coating of the PLGA and CHI layers, the Mg-based micromotor could maintain the Janus microstructure. The Dox/Cur-loaded Mg-based micromotors consisted of a Mg core, a Cur-loaded PLGA layer and a Dox-loaded CHI layer. According to Fig. S2,† the average size of the spherical Mg cores in the micromotors was about 25 μm. After PLGA and CHI coating, the formed Mg/PLGA and Mg/PLGA/CHI micromotors exhibited a rough surface and larger size distribution. Compared with the Mg core, the coating of the PLGA layer caused an increase in size of the Mg/PLGA micromotors with a distribution of 30 ± 5 μm. Meanwhile, the size of the Mg/PLGA/CHI micromotor with the additional coating of CHI was about 34 ± 5 μm. The successful loading of the drug layer was also demonstrated by changes in particle size.

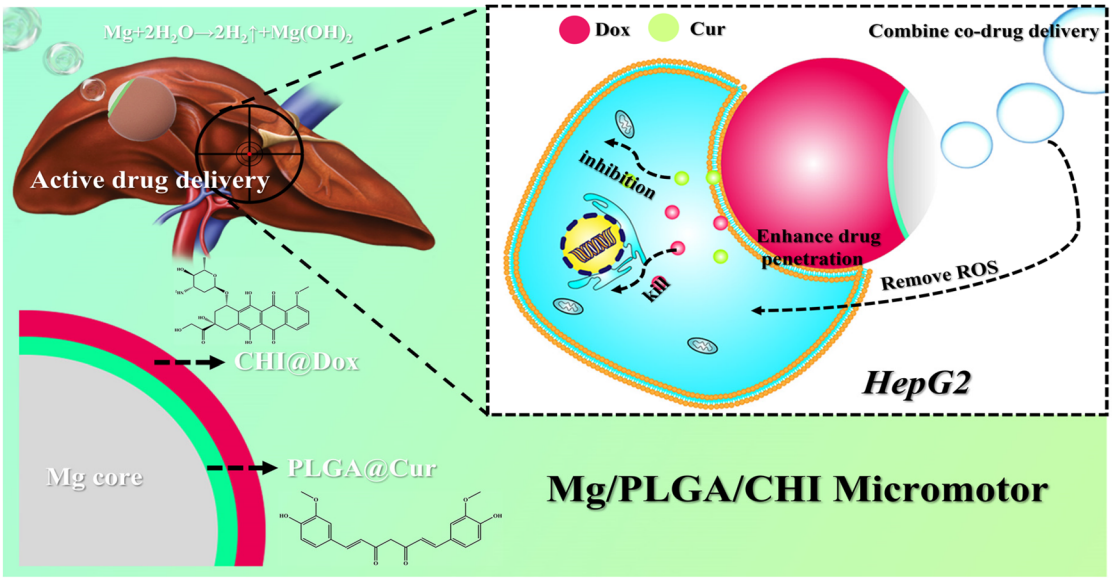

Scheme 1 The mechanism of active drug delivery and combination therapy for the treatment of HepG2 using the Mg/PLGA/CHI micromotor.

After carefully scrapping and collecting from the glass substance (Fig. S3†), a small opening was formed at the contact point of the Mg microparticles and the glass surface, which is essential for the Mg-H_2O reaction. The hydrogen microbubbles generated from this small opening led to micromotor propulsion in the cell culture medium. As seen in Fig. 1a, a small opening of about 10 μm could be found on the bottom side of each micromotor. Energy Dispersive X-ray Spectrometry (EDS) of this individual micromotor further confirmed the Janus structure of the micromotor. A spherical elemental distribution of Mg was observed. The elemental distributions of C and O were uneven, and less elements were observed at the bottom. This is due to the asymmetric distribution of the polymer layer structure. Due to the autofluorescence of Dox and Cur, the PLGA layer loaded with Cur and the CHI layer loaded with Dox were tested under excitation at 470 nm and 560 nm using an inverted fluorescence microscope, respectively. Strong signals of red (Dox) and green (Cur) fluorescence are observed in Fig. 1b, which confirms the successful loading of the drugs on the respective polymer layers. Further, the uniform distribution of the fluorophores confirm that the drugs loaded were uniformly distributed. In summary, all these results show that the Janus-structured Mg/PLGA/CHI micromotor was successfully fabricated and was capable of loading two drugs.

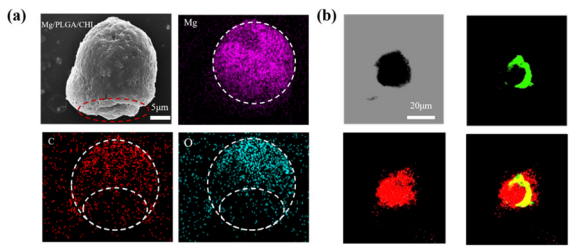

Fig. 1 Characterization of the Mg micromotor. (a) The SEM image of the Mg/PLGA/CHI micromotor and the energy-dispersive X-ray spectroscopy (EDS) results for the distribution of Mg, C, and O in the micromotors. (b) The optical image, fluorescence images and merged image of the drug-loaded Mg/PLGA/CHI micromotor.

The motion of Mg-based micromotors usually relies on the reaction thrust of the H_2 microbubbles coming from the small opening. However, the Mg-H_2O reaction would not provide constant H_2 bubbles because the insoluble Mg $(OH)_2$ passivation layer formed at the small opening might stop the consistent movement. A medium containing HCO_3^{2-} over 100 mM can pierce the Mg $(OH)_2$ passivation layer and accelerate the reaction.[36] In the drug delivery system, the motion of the micromotors can also be affected by the simulated body fluid, which is a complex component.[37] Here, Dulbecco's Modified Eagle medium (DMEM) containing $NaHCO_3$ was chosen as the moving medium, and the magnesium hydroxide passivation layer on the surface of the micromotor was rapidly dissolved under the action of the hydrogen carbonate ions. As illustrated in Fig. 2a and b, after a spontaneous redox reaction between the uncovered Mg cores and the culture medium, the H_2 microbubbles generated from small opening give a recoil force to propel the micromotors forward. Due to the minor differences in the small opening between the micromotors, the ejected microbubbles from the micromotors lead to distinctive motion behaviours (Videos S1 and S2†).[38] The Mg micromotor is propelled by the bubbles ejected from the reaction of the Mg core with the bio-medium and moves in random patterns unless magnetic control is applied by them coating with an Ni or Fe layer.[39,40] Spiral or linear motion behaviours were observed. For the Mg/PLGA micromotors, the same motion modes could also be found, as seen in Fig. S4.† The Janus PLGA layer not only led to directional motility but also enables

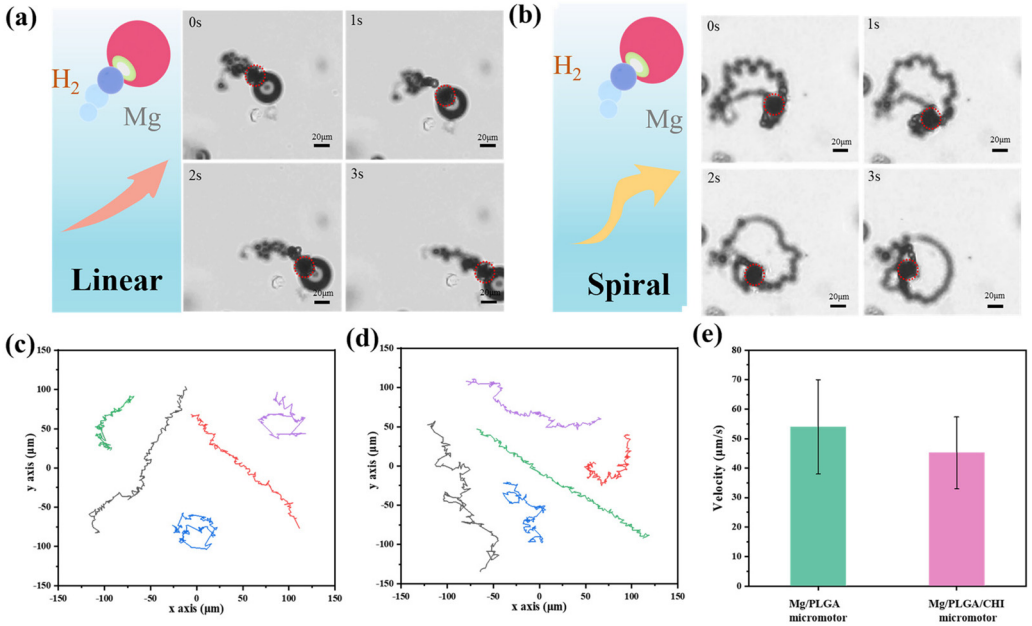

Fig. 2 The motion of the Mg micromotors. (a) The linear motion pattern of the Mg/PLGA/CHI micromotor with a time interval of 3 s. (b) The spiral motion pattern of the Mg/PLGA/CHI micromotor with a time interval of 3 s. The representative tracking trajectories of the (c) Mg/PLGA micromotors (d) Mg/PLGA/CHI micromotors over 6 s in the cell culture medium supplied with 0.3 M $NaHCO_3$ and 0.1 wt% SDS. (e) Comparison of the velocity of the Mg/PLGA micromotors and Mg/PLGA/CHI micromotors.

a controlled of corrosion reaction of the Mg cores. Compared with the short lifetime of pure Mg particles (2–3 min), the lifetime of the Mg/PLGA/CHI micromotors was extended to approximately 10 min (Fig. S5†). It was noticed that H_2 generated during the motion could scavenge ROS by reacting with the noxious $^{\bullet}OH$ species. Meanwhile, the produced H_2 has been shown to have anti-inflammatory, anti-apoptotic and anti-tumor effects.[41,42] Currently, hydrogen produced by Mg-based micromotors is primarily used for ROS elimination in tumor settings and rheumatoid arthritis.[37,43] The optical images of empty PLGA/CHI layers (Fig. S6 and Video S3†) demonstrated that Mg had completely dissolved after successive H_2 releases. The representative tracking trajectories of the Mg/PLGA micromotors and Mg/PLGA/CHI micromotors are respectively presented in Fig. 2c and d. The Mg/PLGA/CHI micromotor had two motion modes over a period of 6 s, and the motion distance was longer. As displayed in Fig. 2e, the velocity of the Mg/PLGA/CHI micromotors decreased to 45 μm s^{-1} due to the loading of the additional CHI layer compared with that of the single-layered micromotors (55 μm s^{-1}), confirming that coating has a slight influence on propulsion during drug delivery. Overall, these results provide solid evidence for an active drug transport process.

Embedding one hydrophilic or hydrophobic drug in the micromotor delivery system cannot satisfy the requirements of significant diagnosis and therapy. As for HCC treatment, combination therapy with different drugs delivered through nanocarriers has become an effectively therapeutic method, as evidenced by the co-delivery of Dox and sorafenib or the combined therapy of Cur and miR-34a.[8,44] Here, the combination of hydrophobic Dox and hydrophilic Cur was achieved by coating two polymers on Mg micromotors (as shown in Fig. 3a). PLGA, a biocompatible polyester, was used as the drug carrier of Cur due to its biodegradability and low cytotoxicity.[46] CHI is a non-toxic polysaccharide with biocompatibility and antibacterial properties and was ideal for loading Dox.[46] Furthermore, the oppositely charged polymers anionic PLGA and cationic CHI could realize electrostatic complexation with each other. In addition, the compact coating of the CHI

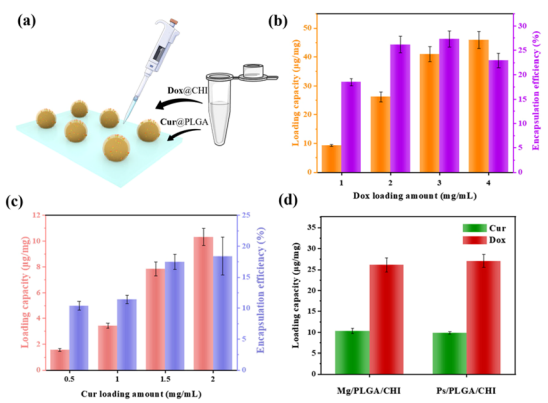

Fig. 3 Encapsulation of Dox and Cur in the micromotors. (a) Schematic the of drug-loading process on the micromotor. The loading capacity and encapsulation efficiency of (b) Cur and (c) Dox under different coating concentrations. (d) Differences in drug-loading capacity between the Mg/PLGA/CHI micromotors and the Ps/PLGA/CHI microparticles.

and PLGA layers also helped avoid burst release of the drugs. To quantify the drug loading capacity and encapsulation efficiency of the micromotors, the standard concentration curves were firstly determined (Fig. S7†). Then, different concentrations of Dox and Cur were coated onto the Mg/PLGA/CHI micromotors to optimize the drug loading amount and coordinate the loading ratio of the two drugs. By testing different concentrations of Dox from 1 to 4 mg mL^{-1} in the chitosan-Dox aqueous solution, the dose of Dox per 1 mg micromotor was be designed from 10 to 40 μg mg^{-1}. However, the corresponded encapsulation efficiency didn't improve with the rise is Dox concentration. When the concentration of Dox was 4 mg mL^{-1}, the encapsulation efficiency was about 22.5% lower than that at 3 mg mL^{-1} (27%) (Fig. 3b). The decrease in efficiency may be due to a larger loss during the coating process (Fig. S3†). With respect to Cur loading, concentration dependence of the loading capacity and encapsulation efficiency was observed in the range from 0.5 to 2 mg mL^{-1} Cur solution. However, although the encapsulation efficiency increased with increasing Cur concentration, the loading capacity and encapsulation efficiency were much lower than that of Dox (Fig. 3c). As shown in Fig. 3b and c, at 1 mg mL^{-1} chitosan-Dox and PLGA-Cur coating solution, the loading capacity of Dox was about 10 μg mg^{-1} and the encapsulation efficiency was about 17%, which are much higher than the Cur loading capacity of about 4 μg mg^{-1} and encapsulation efficiency of about 10%. The difference may result from the large aggregation of Cur at the contact point between Mg and the glass substrate. It is known that the appropriate drug ratio of Dox and Cur is about 2 : 1.[47] The dosage of Cur was calculated according to the optimal proportion based on the clinical requirement of DOX.[48,49] Meanwhile, the loading capacity of Dox and Cur were about 25 μg mg^{-1} and 10 μg mg^{-1} at the concentration of 2 mg mL^{-1} Dox and Cur, which is similar to the appropriate drug ratio. Therefore, Mg/PLGA/CHI micromotors loaded with 25 μg mg^{-1} Dox and 10 μg mg^{-1} Cur were used for subsequent *in vitro* cancer cell treatment. In order to evaluate the active drug delivery competency of the micromotor, inert Ps/PLGA/CHI microparticles were used as the control group. As shown in Fig. 3d, the respective loading capacity of Dox and Cur in the Mg/PLGA/CHI micromotors and Ps/PLGA/CHI was about 10 μg mg^{-1} and 25 μg mg^{-1} with minimal differences.

Micro/nanomotors are capable of enhancing drug delivery to tumors because of their active transport ability, which leads to higher cellular uptake.[42] After loading the drugs on the micromotors at levels close to the optimal proportional load, the uptake of Dox and Cur in HepG2 cells due to the motion of the Mg/PLGA/CHI micromotors was detected by the intrinsic fluorescence of DOX (red) and Cur (green). As demonstrated in Fig. 4a, Dox and Cur were efficiently absorbed by HepG2 cells after 1 h of incubation. However, low fluorescence intensity was observed in the Ps/PLGA/CHI group. This result indicates that the accelerated mass transfer resulting from the active motion of the micromotors could improve the uptake of Dox and Cur by the HepG2 cells. Compared with the inert Ps/PLGA/CHI group, the absorption of Dox was about 2.9 times stronger (Fig. 4b). While, the fluorescence intensity of Cur was intensified by about 1.5 times (Fig. 4c). The different release rates may be due to the different release sequence of the two polymer-coated drugs. The release of Cur from the PLGA inner layer requires the degradation of the CHI layer or the depletion of the Mg core. Apart from the co-delivery of drugs, H_2 released from the small opening could also enter the cellular interior. Previous studies have shown that hydrogen produced by magnesium inhibit the growth of cancer cells mainly by reacting with harmful $^{\cdot}OH$ to remove ROS.[37,50] To evaluate the ROS-scavenging ability of the micromotor (Fig. S7†), an ROS probe (DCFH-DA) was used to detect the intracellular ROS levels. DCFH-DA can penetrate the cells, where it is then degraded by intracellular lipases and gets converted into DCFH. The formed DCFH can be further oxidized to fluorescent DCF, so the fluorescence intensity positively correlates with the intracellular ROS level. As seen in Fig. 5, the fluorescence intensity of the HepG2 cells decreased with the increase in Mg/PLGA/CHI micromotor and Mg particle quantity, confirming that active H_2 can remove overexpressed ROS in HepG2 cells. The Mg/PLGA/CHI micromotors present a stronger ROS removal capability compared with naked Mg microparticles due to the continuous generation of hydrogen and the ability to release H_2 instantly and quickly. It has been confirmed earlier that hydrogen produced by the the Mg/PLGA/CHI micromotors can break the uniform balance of redox and lead to apoptosis of cancer cells.[37]

Compared with single drug administration, combined therapy is one of the ways to overcome multidrug resistance

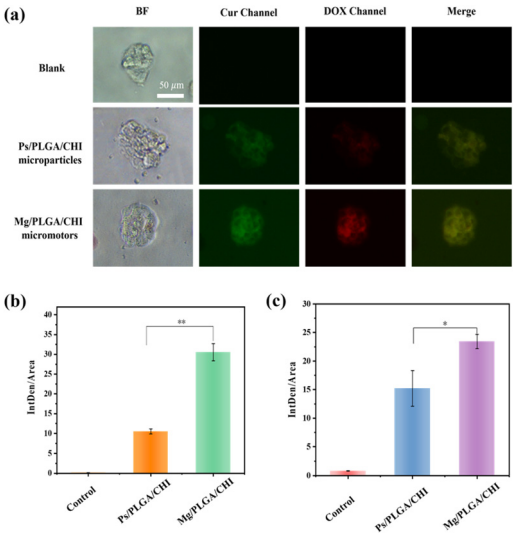

Fig. 4 Measurement of Dox/Cur uptake efficacy of cancer cell. (a) Optical and florescence images after culture of drug-loaded Ps/PLGA/CHI micromotors and drug-loaded Mg/PLGA/CHI micromotors with HepG2 cells. The calculated fluorescence intensity of (b) Dox and (c) Cur in HepG2 cells after treatment with drug-loaded Ps/PLGA/CHI micromotors and drug-loaded Mg/PLGA/CHI micromotors. (The symbol * indicates the statistical significance at level of $P < 0.05$ and ** indicates $P < 0.01$.)

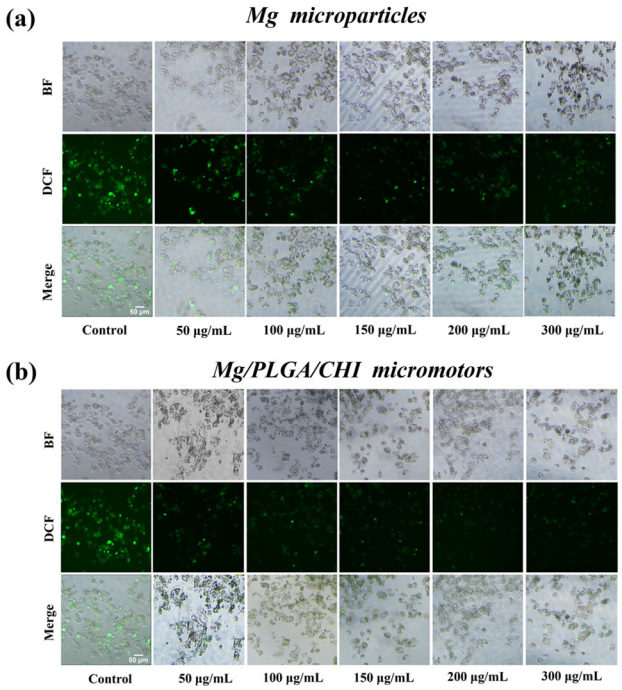

Fig. 5 The ROS-scavenging ability of the (a) Mg microparticles and (b) Mg/PLGA/CHI micromotors in HepG 2 cells after treatment, as detected by DCFH-DA.

and improve the bioavailability of drugs to cancer cells.[5] It is known that the movement of micromotors accelerates the permeability and absorption of drugs into cells.[24] To evaluate the anticancer effect of the combination treatment, the proliferation inhibition and live/dead staining of HepG2 cells after treatment with Mg/PLGA/CHI micromotors with/without drugs were performed. The therapeutic effects of free Dox, free Cur, and the Dox/Cur mixture on HepG2 cells were first quantified after co-culturing them for 24 h. Dox is a common chemotherapeutic drug that works by intercalating with the DNA and inhibiting macromolecular biosynthesis in the nuclei.[44] Meanwhile, Cur mainly relies on its natural antioxidant activity and interferes with topoisomerase II-mediated DNA cleavage in the cytoplasm.[45] As shown in Fig. 6a, the inhibitory effect of the free drugs on cell proliferation was concentration-dependent in the ranges of 2.5 μg mL^{-1}–40 μg mL^{-1} Dox and 1.25 μg mL^{-1}–20 μg mL^{-1} Cur. The synergistic effect of Cur and Dox was most significant at a Cur concentration of 10 μg mL^{-1} and Dox concentration of 20 μg mL^{-1}. However, the inhibitory effect of the Dox-Cur mixture on cell proliferation was slightly improved, and it was roughly lower than that of Dox in the other groups. The reason may be that only one drug plays a dominant role when the Cur concentration is too low or the Dox concentration is too high, leading to insignificant synergy between the two. In spite of the slight enhancement, the addition of Cur can reduce the emergence of drug resistance and contribute to the alleviation of damage to normal cells.[5] Next, we tested the cytotoxicity of the Mg microparticles and Mg/PLGA/CHI micromotors at concentrations ranging from 0.25 mg mL^{-1} to 2 mg mL^{-1}, and no significant cytotoxicity was observed (Fig. 6b). In particular, compared with the inert Ps/PLGA/CHI particles, at the concentration of 1 mg mL^{-1}, the antitumor activity of the micromotors was significantly

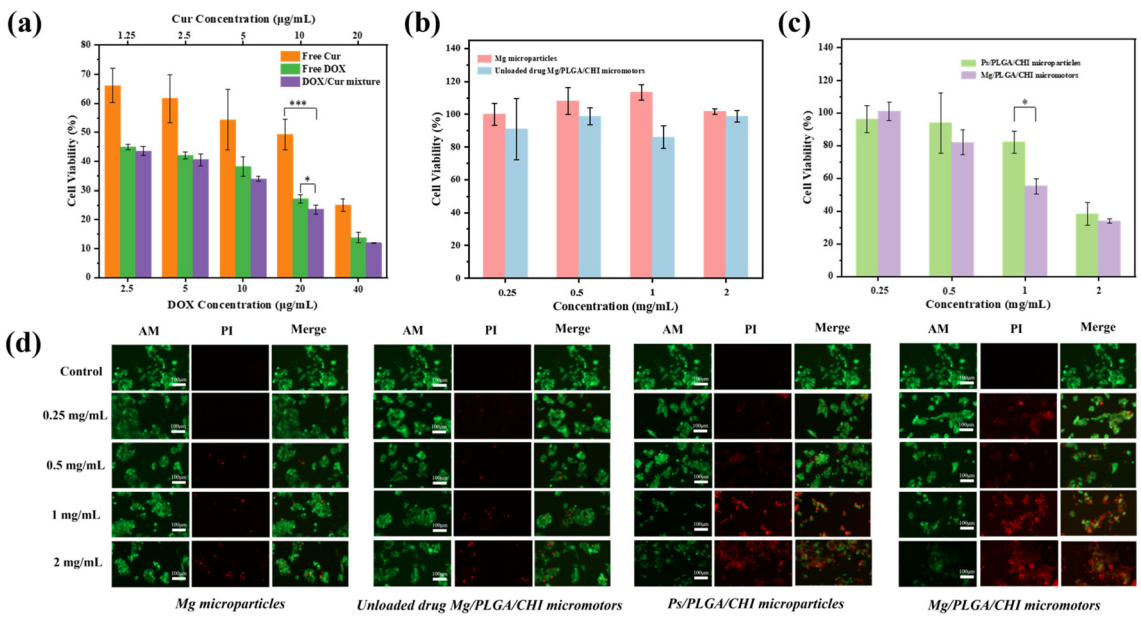

Fig. 6 Synergistic therapeutic effect of Mg-based motors *in vitro*. (a) Cytotoxicity of free drugs and the free drug mixture. (b) Cytotoxicity of the Mg microparticles, unloaded Mg/PLGA/CHI micromotors. (c) Cytotoxicity of the drug-loaded Ps/PLGA/CHI microparticles and Mg/PLGA/CHI micromotors. (d) Live/dead staining of the Mg microparticles, unloaded Mg/PLGA/CHI micromotors, and drug-loaded Ps/PLGA/CHI microparticles and Mg/PLGA/CHI micromotors. (The symbol * indicates the statistical significance at level of $P < 0.05$ and *** indicates $P < 0.001$.)

improved. Cell proliferation was almost as low as 50% at this concentration, which is a significant reduction by 30% compared with the inert group. However, when the concentration of the drug carrier was low, the drug loaded on the micromotors was too less to effectively kill the cancer cells. Meanwhile, when the concentration of the drug carrier was high, the effect of the chemical drug treatment was dominant, and the advantage of active drug delivery was less significant (Fig. 6c). The huge decrease in cell proliferation between the active and inert groups confirmed the significantly improved effect of micromotors. As per the previous study, the degradation process of the PLGA/CHI layer can take more than 3 days.[51] The drugs are first released through the pores formed in the layers, dependent on their active diffusion during locomotion. After the motion of micromotors stops, polymer degradation along with continued drug release occurs. After 24 h in culture with the co-drug delivery by the micromotors, the proliferation inhibition of HepG2 was higher than those with the free drugs, which may have resulted from enhanced drug adsorption and the unreleased drugs in the polymer layers. The CHI layer is a positive polymer that can attach to tumors through motion in tumor ascites. As shown in Fig. 6d, the same live/dead staining was applied to these four groups. After treatment with the Mg microparticles and Mg/PLGA/CHI micromotors, nearly no dead cells were observed at low concentrations. However, dead cells were found at the concentrations of 1 mg mL^{-1} and 2 mg mL^{-1}, which may be ascribed to the autonomous drive process of the micromotor to produce hydrogen. Meanwhile, the active combined drug delivery system showed a higher antitumor activity. The strongest red fluorescence was observed in the co-drug active groups at the concentration of 1 mg mL^{-1}, and at the concentration of 2 mg mL^{-1}, little green fluorescence could be seen, indicating the total apoptosis of cancer cells.

Experimental details

Materials and reagents

Mg microparticles (average size: 25 ± 5 μm) were obtained from TangShan WeiHao Magnesium Powder Co., Ltd. Poly (lactic-*co*-glycolic acid) (PLGA, 8000 Da) was acquired from Jinan Daigang Biomaterial Co., Ltd. Poly(vinylpyrrolidone) (PVP-K30) was purchased from Beijing Solarbio Science & Technology Co., Ltd. Methylene blue (MB), sodium dodecyl sulfate (SDS) and dimethyl sulfoxide (DMSO) were obtained from Sinopharm Chemical Regents Co., Ltd. Doxorubicin (Dox) and curcumin (Cur) were purchased from Sigma Aldrich. Polystyrene (Ps) microspheres were purchased from Wuxi Ruige Biotechnology Co., Ltd. The Cell Counter kit-8 (CCK-8) and calcein *O*,*O*′-diacetate tetrakis(acetoxymethyl) ester/propidium iodide (calcein-AM/PI) were obtained from Dojindo Laboratories (Kumamoto, Japan). 2,7-Dichlorodihydrofluorescein diacetate (DCFH-DA) was obtained from Beyotime Biotechnology. Hepatoma carcinoma cells (HepG 2) were obtained from American Type Culture Collection (ATCC). All reagents for cell culture were bought from Gibco. Ultra-pure water (18.2 MΩ cm) was used for solution preparation. All reagents were used as received without further treatment.

Fabrication of the Mg/PLGA/CHI micromotors

The Mg microparticles were washed with acetone three times to eliminate impurities before drying them in a vacuum at room temperature. Then, 60 μL of polyvinyl pyrrolidone was dropped on a glass slide and dried at 60 °C, and the Mg microspheres were spread on the glass substrate (~2 mg per glass slide). The glass substrate was further kept under a relative humidity of 50% for 30 min, and then, the Mg cores were partially embedded into a swelled PVP film and fixed in a humid environment. Then, 120 μL 1% PLGA ethyl acetate solution was dropped on the glass substrate and dried naturally. A homogeneous PLGA coating was formed over the exposed surfaces of the Mg cores due to the rapid volatilization of ethyl acetate. Then, another 60 μL PLGA ethyl acetate solution containing different contents of Cur was dropped on the glass substance. Then, 100 μL 0.05% CHI with different concentrations of Dox was dropped to the glass substance in the same way and dried at 37 °C under oscillation. Finally, micromotors loaded with the drugs (Mg/PLGA/CHI) were collected from the slide. The micromotors were gently scraped from the slide during collection. Due to the presence of PVP, the Mg micromotors will have an opening at the contact point between the Mg core and the glass substrate after coating. This small opening is the key point for the micromotor to react with the fuel and drive the autonomous movement. The Mg-based micromotor loaded with Dox and Cur (Mg/PLGA@Cur/CHI@Dox) is denoted as the Mg/PLGA/CHI micromotor.

Characterization of the Mg/PLGA/CHI micromotors

The morphology and element distributions of the Mg/PLGA/CHI micromotors were characterized by using a scanning electron microscope (SEM, JSM-7600F) equipped with an Oxford X-MAX Energy Dispersive X-ray Spectrometer (EDS). The optical and fluorescence images were recorded by an inverted fluorescence microscope (TE2000, Nikon, Japan).

Motion observation of the Mg/PLGA/CHI micromotors

The Dulbecco's Modified Eagle's medium (DMEM, containing 10% fetal bovine serum, 100 μg mL^{-1} penicillin, 100 μg mL^{-1} streptomycin) used for culturing the HepG2 cells was supplemented with 0.3 M $NaHCO_3$ and 0.1% SDS and used as a fuel for the Mg/PLGA/CHI micromotors. The motion videos of the micromotors were recorded under an inverted optical microscope (CKX53, Olympus Instrument Inc., Tokyo, Japan). All the motion videos of the micromotors were analyzed by Video Spot Tracker V08.01 software.

Encapsulation efficiency of Dox and Cur in the micromotors

The standard curves of Dox and Cur were first calculated by using a Shimadzu ultraviolet-visible (UV-vis) spectrophotometer (UV3101PC; Japan) based on the peaks at 480 and 425 nm. Then, for the drug encapsulation study, ~2 mg Dox/

Cur-loaded micromotors were suspended in 2 mL of PBS at 37 °C in a rotary shake. The concentration of released Dox/Cur in the solution was determined by measuring the absorbance at wavelengths 480 and 425 nm, respectively. Finally, the encapsulation efficiency of Dox and Cur in the Mg micromotors was calculated based on the standard curves.

Evaluation of the ROS level

The HepG2 cells were digested and seeded in 96-well plates at a density of 5×10^3 cells per well and cultivated in the DMEM culture medium for 24 h. Then, the medium was replaced with fresh DMEM medium containing 0.3 M $NaHCO_3$ along with Mg particles or Mg/PLGA/CHI micromotors at the concentrations of 0, 25, 50, 100, 150, 200 and 300 μg mL^{-1}, respectively, and incubated for 2 h. After the culture process, the DCFH-DA probe was added into each well to detect the intracellular ROS level. The fluorescence images were obtained using an inverted fluorescence microscope (TE2000, Nikon, Japan).

Evaluation of the Dox/Cur uptake efficacy

The HepG2 cells were seeded in 24-well plates at a density of 5×10^5 cells per well and cultivated in 1 mL DMEM culture medium for 24 h. Inert Ps microspheres loaded with Dox and Cur (Ps/PLGA/CHI) were used as the control. The spent culture medium was replaced by fresh DMEM containing 0.3 M $NaHCO_3$ and co-cultured for 1 h with 500 μg mL^{-1} Mg/PLGA/CHI micromotors and Ps/PLGA/CHI microparticles. Finally, the fluorescence images were taken under a fluorescence microscope. Meanwhile, the semiquantitative analysis of the average fluorescence intensity per unit area of Dox and Cur absorption was conducted.

Cytotoxicity analysis

The cytotoxicity analysis of HepG2 cells was performed using the same cell density and incubation time measured in the ROS evaluation experiment. Then, the culture medium was replaced with fresh DMEM culture medium containing Mg microparticles, unloaded Mg/PLGA/CHI micromotors, and drug-loaded Ps/PLGA/CHI microparticles and Mg/PLGA/CHI micromotors. After another 24 h of incubation, the medium from all the well plates was removed. The CCK-8 medium was added and incubated for 2 h. The absorbance of CCK-8 was measured using a microplate reader. Cell viability was calculated by using the following equation:

$$\text{Cell viability}(\%) = \frac{A_2 - A_1}{A_3 - A_1} \times 100\%$$

where A_1 is the OD value of the blank control group, A_2 is the OD value of the experimental group, and A_3 is the OD value of the negative control group.

In the same way, the live/dead cell experiments were conducted by using two staining reagents, namely AM and PI. The cells mixed with Mg microparticles, unloadedMg/PLGA/CHI micromotors, and drug-loaded Ps/PLGA/CHI microparticles and Mg/PLGA/CHI micromotors were incubated for 24 h. The AM/PI solution was added and incubated for 0.5 h, and the cells were taken out for fluorescence microscopic observation.

Conclusions

Overall, we have demonstrated a biocompatible combination drug delivery platform made of Mg/PLGA/CHI micromotors to improve therapeutic efficacy and enhance drug permeability in HCC. The micromotor drug delivery platform exhibits good movement behaviour and multi-drug loading capacity. By optimizing the drug loading ratio, the ideal loading capacity of Cur and Dox was found to be 10 μg mg^{-1} and 25 μg mg^{-1}, respectively. H_2 produced during active administration of the platform in the medium could also reduce the intracellular ROS concentration and inhibits tumor growth. In the HepG2 cell culture, the combined drug delivery motor shows significantly enhanced drug permeability compared with the passive group. The intracellular fluorescence signals of the drugs Dox and Cur were 2.9 and 1.5 times higher than that of the inert group. Moreover, the antitumor activity was significantly higher by 30% than that in the inert group when the co-culture drug concentration reached 1 mg mL^{-1}. Due to the synergistic effect of Dox and Cur, the HepG2 cells showed obviously inhibited proliferation and apoptosis compared with single drug treatment. Overall, the active drug delivery system presented successful loading of the hydrophilic and hydrophobic drugs independently at the same time, enhanced cell penetration, promoted drug absorption, ROS elimination and inhibited tumor cell proliferation, providing an effective plan for HCC treatment. Taking into account the acidic tumor microenvironment, pH-sensitive coatings can support further enhancement in the delivery of multiple drugs. At present, micro/nanomotors are gradually being developed and employed in the mouse tumor environment, including the application of Mg micromotors to improve the survival rate of tumor mice.[24,52,53] Unlike *in vitro* cellular levels, it is difficult to maintain high concentrations of free drugs in and around cancer cells in the body. Therefore, the development of diverse drug delivery vehicles is necessary.[52,53] Compared to the passive phases of drug delivery, the active phases of drug administration, which rely on the autonomous motion capability and delicate functional design of micro/nanomotors, are expected to exert enhanced antitumor effects when further applied in *in vivo* therapy.[54] We envision that the proposed Mg-based micromotor drug delivery platform would have great potential in diverse biomedical applications.

Author contributions

Qingtao Song and Yilin Liu contributed equally to this work. Qingtao Song: methodology, writing – original draft. Yilin Liu: investigation, writing – original draft. Xiaoyong Ding: data curation. Miao Feng: data curation. Jing Li: resources. Wenjuan Liu: supervision, writing – review & editing. Bohan Wang: writing – review & editing. Zhongwei Gu: supervision.

Conflicts of interest

All authors declare no conflicts of interest.

Acknowledgements

This work was supported by Natural Science Foundation of Jiangsu Province (BK20211265), the National Natural Science Foundation of China (No. 22178306), Fundamental Research Funds for the Central Universities (2020BCE006), the PAPD-A Project Funded by the Priority Academic Program Development of Jiangsu Higher Education Institutions. The authors acknowledge Suqian Advanced Materials Industry Technology Innovation Center of Nanjing Tech University for support.

References

1 A. Villanueva and J. M. Llovet, *Gastroenterology*, 2011, **140**, 1410–1426.
2 J. M. Llovet and J. Bruix, *Hepatology*, 2008, **48**, 1312–1327.
3 K. M. Schneider, A. Mohs, W. Gui, E. J. C. Galvez, L. S. Candels, L. Hoenicke, U. Muthukumarasamy, C. H. Holland, C. Elfers, K. Kilic, C. V. Schneider, R. Schierwagen, P. Strnad, T. H. Wirtz, H. Marschall, E. Latz, B. Lelouvier, J. Saez-Rodriguez, W. de Vos, T. Strowig, J. Trebicka and C. Trautwein, *Nat. Commun.*, 2022, **18**, 1–19.
4 J. B. Sun, J. H. Duan, S. L. Dai, J. Ren, Y. D. Zhang, J. S. Tian and Y. Li, *Cancer Lett.*, 2007, **258**, 109–117.
5 X. Zhao, Q. Chen, W. Liu, Y. Li, H. Tang, X. Liu and X. Yang, *Int. J. Nanomed.*, 2015, **10**, 257–270.
6 U. Asghar and T. Meyer, *J. Hepatol.*, 2012, **56**, 686–695.
7 F. Zhang, Y. Jia, X. Zheng, D. Shao, Y. Zhao, Z. Wang and L. Chen, *Acta Biomater.*, 2019, **100**, 352–364.
8 B. F. Far, M. R. Naimi-Jamal, H. Daneshgar and N. Rabiee, *Environ. Res.*, 2023, **225**, 115589.
9 G. Minotti, P. Menna, E. Salvatorelli, G. Cairo and L. Gianni, *Pharmacol. Rev.*, 2004, **56**, 185–229.
10 A. C. Ketron, O. N. Gordon, C. Schneider and N. Osheroff, *Biochemistry*, 2013, **52**, 221–227.
11 S. Ganta and M. Amiji, *Mol. Pharm.*, 2009, **6**, 928–939.
12 X. Fan, C. Zhang, D. B. Liu, J. Yan and H. P. Liang, *Curr. Pharm. Des.*, 2013, **19**, 2011–2031.
13 C. Loo, D. Traini, P. M. Young, T. Parumasivam and W. Lee, *J. Drug Delivery Sci. Technol.*, 2023, **82**, 104375.
14 X. Duan, J. Xiao, Q. Yin, Z. Zhang, H. Yu, S. Mao and Y. Li, *ACS Nano*, 2013, **7**, 5858–5869.
15 Z. Zhang and S. Song, *Biomaterials*, 2017, **132**, 16–27.
16 Y. Lu, T. Xiao, R. Lai, Z. Liu, W. Luo, Y. Wang, S. Fu, G. Chai, J. Jia and Y. Xu, *Pharmaceutics*, 2023, **15**, 1500.
17 T. Xu, W. Gao, L. Xu, X. Zhang and S. Wang, *Adv. Mater.*, 2017, **29**, 1603250.
18 T. Li, J. Li, K. I. Morozov, Z. Wu, T. Xu, I. Rozen, A. M. Leshansky, L. Li and J. Wang, *Nano Lett.*, 2017, **17**, 5092–5098.
19 F. Zhang, Z. Li, Y. Duan, A. Abbas, R. Mundaca-Uribe, L. Yin, H. Luan, W. Gao, R. H. Fang, L. Zhang and J. Wang, *Sci. Robot.*, 2022, **7**, eabo4160.
20 L. Kong, N. Rohaizad, M. Z. M. Nasir, J. Guan and M. Pumera, *Anal. Chem.*, 2019, **91**, 5660–5666.
21 T. G. Leong, C. L. Randall, B. R. Benson, N. Bassik, G. M. Stern and D. H. Gracias, *Proc. Natl. Acad. Sci. U. S. A.*, 2009, **106**, 703–708.
22 M. Zhou, Y. Xing, X. Li, X. Du, T. Xu and X. Zhang, *Small*, 2020, **16**, 2003834.
23 Y. Xing, M. Zhou, X. Liu, M. Qiao, L. Zhou, T. Xu, X. Zhang and X. Du, *Chem. Eng. J.*, 2023, **461**, 142142.
24 C. Wang, B. E. F. de Ávila, R. Mundaca-Uribe, M. A. Lopez-Ramirez, D. E. Ramírez-Herrera, S. Shukla, Ni. F. Steinmetz and J. Wang, *Small*, 2020, **16**, 1907150.
25 Z. Xiao, S. Duan, P. Xu, J. Cui, H. Zhang and W. Wang, *ACS Nano*, 2020, **14**, 8658–8667.
26 C. M. Oral, M. Ussia, M. Urso, J. Salat, A. Novobilsky, M. Stefanik, D. Ruzek and M. Pumera, *Adv. Healthcare Mater.*, 2022, **11**, 2202682.
27 X. Lu, H. Shen, Y. Wei, H. Ge, J. Wang, H. Peng and W. Liu, *Small*, 2020, **16**, 2003678.
28 X. Li, Y. Zhao, D. Wang and X. Du, *Colloids Surf., A*, 2023, **658**, 130712.
29 Q. Song, X. Ding, Y. Li, W. Liu, J. Li, B. Wang and Z. Gu, *Appl. Mater. Today*, 2023, **31**, 101779.
30 K. Liu, Q. Liu, J. Yang, C. Xie, S. Wang, F. Tong, J. Gao, L. Liu, Y. Ye, B. Chen, X. Cai, Z. Liu, Z. Li, F. Peng and Y. Tu, *ACS Nano*, 2023, **17**, 300–311.
31 F. Mou, C. Chen, Q. Zhong, Y. Yin, H. Ma and J. Guan, *ACS Appl. Mater. Interfaces*, 2014, **6**, 9897–9903.
32 T. Maric, S. Atladóttir, L. H. E. Thamdrupa, O. Ilchenkoa, M. Ghavami and A. Boisen, *Appl. Mater. Today*, 2022, **27**, 101418.
33 B. E. F. de Ávila, M. A. Lopez-Ramirez, R. Mundaca-Uribe, X. Wei, D. E. Ramírez-Herrera, E. Karshalev and J. Wang, *Adv. Mater.*, 2020, **32**, 2000091.
34 H. Zhou, Y. Yuan, Z. Wang, Z. Ren, M. Hu, J. Lu, H. Gao, C. Pan, W. Zhao and B. Zhu, *Colloids Surf., A*, 2023, **658**, 130654.
35 X. Zhang, X. Chen, B. Li, S. Xu, Z. Wu, M. Hu, Z. Zhao, G. Zhao, C. Wang, W. Hong, S. Li, L. Li, C. Wang, G. Nie and R. Liu, *Biomaterials*, 2022, **281**, 121362.
36 F. Mou, C. Chen, Q. Zhong, Y. Yin, H. Ma and J. Guan, *ACS Appl. Mater. Interfaces*, 2014, **6**, 9897–9903.
37 K. Liu, J. Ou, S. Wang, J. Gao, L. Liu, Y. Ye, D. A. Wilson, Y. Hua, F. Peng and Y. Tu, *Appl. Mater. Today*, 2020, **20**, 100694.
38 Z. Wang, S. Wang, K. Liu, D. Fu, Y. Ye, J. Gao, L. Liu, D. A. Wilson, Y. Tu and F. Peng, *Appl. Mater. Today*, 2020, **21**, 100839.
39 S. S. Das, S. Erez, E. Karshalev, Y. Wu, J. Wang and G. Yossifon, *ACS Appl. Mater. Interfaces*, 2022, **14**, 30290–30298.

40 Z. Wu, B. E. F. de Ávila, A. Martín, C. Christianson, W. Gao, S. K. Thamphiwatana, A. Escarpa, Q. He, L. Zhang and J. Wang, *Nanoscale*, 2015, **7**, 13680–13686.
41 Y. Wu, M. Yuan, J. Song, X. Chen and H. Yang, *ACS Nano*, 2019, **13**, 8505–8511.
42 T. Zhang, Y. Wang, R. Li, J. Xin, Z. Zheng, X. Zhang, C. Xiao and S. Zhang, *Acta Biomater.*, 2023, **158**, 475–492.
43 C. Xu, S. Wang, H. Wang, K. Liu, S. Zhang, B. Chen, H. Liu, F. Tong, F. Peng, Y. Tu and Y. Li, *Nano Lett.*, 2021, **21**, 1982–1991.
44 N. A. Abtahi, S. M. Naghib, S. J. Ghalekohneh, Z. Mohammadpour, H. Nazari, S. M. Mosavi, S. M. Gheibihayat, F. Haghiralsadat, J. Z. Reza and B. Z. Doulabi, *Chem. Eng. J.*, 2022, **429**, 132090.
45 J. Zimmermann, N. Jürgensen, A. J. Morfa, B. Wang, S. Tekoglu and G. Hernandez-Sosa, *ACS Sustainable Chem. Eng.*, 2016, **4**, 7050–7055.
46 Q. Chen, Y. Qi, Y. Jiang, W. Quan, H. Luo, K. Wu, S. Li and Q. Ouyang, *Mar. Drugs*, 2022, **20**, 536.
47 Y. Zhang, C. Yang, W. Wang, J. Liu, Q. Liu, F. Huang, L. Chu, H. Gao, C. Li, D. Kong, Q. Liu and J. Liu, *Sci. Rep.*, 2016, **6**, 1–12.
48 J. J. Luke, D. R. D'Adamo, M. A. Dickson, M. L. Keohan, R. D. Carvajal, R. G. Maki, E. de Stanchina, E. Musi, S. Singer and G. K. Schwartz, *Clin. Cancer Res.*, 2012, **18**, 2638–2647.
49 A. Burroughs, D. Hochhauser and T. Meyer, *Lancet Oncol.*, 2004, **5**, 409–418.
50 N. Yang, F. Gong, B. Liu, Y. Hao, Y. Chao, H. Lei, X. Yang, Y. Gong, X. Wang, Z. Liu and L. Cheng, *Nat. Commun.*, 2022, **13**, 2336.
51 S. Jung, G. H. Yoon, H. C. Lee, M. H. Jung, S. I. Yu, S. J. Yeon, S. K. Min, Y. S. Kwon, J. H. Hwang and H. S. Shin, *Sci. Rep.*, 2015, **5**, 18089.
52 Z. Sun, T. Wang, J. Wang, J. Xu, T. Shen, T. Zhang, B. Zhang, S. Gao, C. Zhao, M. Yang, F. Sheng, J. Yu and Y. Hou, *J. Am. Chem. Soc.*, 2023, **145**, 11019–11032.
53 B. Wang, Y. Qin, J. Liu, Z. Zhang, W. Li, G. Pu, Z. Yuanhe, X. Gui and M. Chu, *ACS Appl. Mater. Interfaces*, 2023, **15**, 2747–2759.
54 A. H. Meisami, M. Abbasi, S. Mosleh-Shirazi, A. Azari, A. M. Amani, A. Vaez and A. Golchin, *Eur. J. Pharmacol.*, 2022, **926**, 175011.